TNIK overexpression is sufficient for chemoradiation resistance in limited-stage small cell lung cancer

Dipanwita Dutta Chowdhury[1,*], Eddie L. Imada[2,3,*], Nick Connis[4,*], Jinhee Chang[1], Aaron Chan[1], Hwai Wei Tseng[1], Audrey Lafargue[1], Francesca A. Carrieri[5], Triet Nguyen[1,6], Danielle N. Waters [1], Elan R. Simms[1], Amol C. Shetty[7], Yang Song[7], Muhammad Ajmal Khan[1], Mohammad Rezaee[5], Phuoc T. Tran[1,5,+], Luigi Marchionni[2,+], Christine L. Hann[4,+]

* - these authors contributed equally
+ - corresponding authors

[1]Department of Radiation Oncology, Division of Translational Radiation Sciences, University of Maryland Baltimore, School of Medicine, Baltimore, Maryland.

[2]Department of Pathology and Laboratory Medicine, Weill Cornell Medicine, New York, New York.

[3]Department of Urology, Johns Hopkins University School of Medicine, Baltimore, Maryland.

[4]Department of Oncology, Johns Hopkins University School of Medicine, Baltimore, Maryland.

[5]Department of Radiation Oncology and Molecular Radiation Sciences, Johns Hopkins University, School of Medicine, Baltimore, Maryland.

[6]Department of Biochemistry and Molecular Biology, Johns Hopkins University, School of Public Health, Baltimore, Maryland.

[7]Institute for Genome Sciences, University of Maryland School of Medicine, Baltimore, Maryland.

Running title: TNIK mediates chemoradiation resistance in LS-SCLC.

Key words: TNIK, limited-stage small cell lung cancer, chemoradiation resistance, patient-derived xenografts, DNA damage response

Additional information:
Corresponding authors:

Christine L. Hann, MD, PhD, Department of Oncology, Johns Hopkins University School of Medicine, Viragh Building Room 8123, 201 N. Broadway St., Baltimore, MD 21287.
Email: chann1@jhmi.edu. Phone: +1 (410) 502 0678
Phuoc T. Tran, MD, PhD, Department of Radiation Oncology, University of Maryland School of Medicine, 850 W. Baltimore Street, Baltimore, MD 21201.
Email: phuoc.tran@som.umaryland.edu. Phone: +1 (346) 725 5816
Luigi Marchionni, MD, PhD, Weill Cornell Medicine, New York, NY.
Email: lum4003@med.cornell.edu. Phone: +1 (646) 962 8767

Conflict of interest disclosure statement: Dr. Hann receives research funding from AbbVie, Amgen, AstraZeneca, Bristol Myers Squibb and Daiichi Sankyo and has consulted for Amgen, AstraZeneca, Genentech, Daiichi Sankyo , Puma Biotechnology,. Dr. Tran has consulted for Natsar Pharmaceuticals and also has a patent (Patent filed 3/9/2012. PCT/US2012/028475. PCT/WO/2012/122471) licensed with royalties to Natsar Pharmaceuticals. Other consulting/advisory role include Regeneron, Dendreon, Noxopharm, Janssen, Myovant Sciences, AstraZeneca, Lantheus and has received research funding from Astellas Pharma, Reflexion Medical, Bayer Health. Dr. Tran also has a patent for 9114158 issued to Natsar Pharmaceuticals with royalties paid from Natsar Pharmaceuticals. The remaining authors have declared no conflict of interest.

Word count: 4820
Number of figures and tables: 14 figures (5 main figures, 9 supplementary figures) and 7 supplementary tables

Abstract

Small cell lung cancer (SCLC) is characterized by early metastasis, intrinsic chemoradiation resistance and tumor recurrence. Besides the lack of potentially targetable oncogenic drivers, therapeutic advancements are also hindered by the scarcity of surgically resected tissue specimens ideal for profiling studies. We used patient-derived xenografts (PDXs) to model SCLC chemoradiation resistance and identified chemoradiation resistance candidate genes using RNA sequencing. Additionally, we used human SCLC cell lines to confirm our *in vivo* results and delineate the underlying mechanism. Transcriptome profiling showed that the Traf2- and Nck-interacting kinase (*TNIK*) gene was consistently upregulated in an array of SCLC PDXs exposed to chemoradiation compared to monotherapy, which is consistent with previous observation of *TNIK* amplification in human samples. Genetic depletion ($p<0.01$) or pharmacological inhibition ($p<0.0001$) of TNIK reduced *in vitro* clonogenic survival of $TNIK^{high}$ SCLC cells and promoted sensitivity to chemoradiation. *In vivo*, pharmacological inhibition of TNIK enhanced chemoradiation sensitivity ($p<0.0001$) of H446 cell line-derived xenograft (CDX) in NOD-SCID mice. Furthermore, pharmacological inhibition of TNIK *in vivo* demonstrated sensitivity ($p<0.0001$) to chemoradiotherapy in LX33 PDX. These results indicate that TNIK plays a role in conferring resistance to chemoradiation in SCLC cell lines and *in vivo* in SCLC CDX and PDX models. Delineating the mechanism behind radiosensitization, suggested that TNIK inhibition may impair the DNA damage response in irradiated cells. Collectively, these findings suggest that TNIK may be a promising therapeutic target in limited-stage (LS) SCLC and support further investigation of TNIK inhibition in combination with standard chemoradiotherapy.

Introduction

Small cell lung cancer (SCLC) represents 15% of all lung cancers. Globally, roughly 250,000 patients are diagnosed with SCLC each year, of which nearly 200,000 die from the disease (1–3). Due to its early propensity for metastasis, all patients—including those with limited-stage (LS) disease, receive systemic chemotherapy (4). In patients with LS-SCLC, etoposide plus a platinum agent (EP) combined with thoracic radiotherapy (TRT), confers a 30-35% 5-year overall survival (OS) and a median survival of 25-30 months (5). More recently, the ADRIATIC trial demonstrated that consolidation with the anti–PD-L1 antibody durvalumab, following completion of chemoradiation, significantly improved 3-year survival (56.5% vs. 47.6% in the durvalumab vs. placebo arms, respectively) and established consolidation durvalumab as a new standard of care (SOC) for patients with LS-SCLC (6). In exploratory analyses, treatment with durvalumab was associated with a reduction in extrathoracic relapse, while the rate of intrathoracic progression remained unchanged (7). This pattern suggests that while immunotherapy may enhance systemic immune surveillance, it does not adequately address residual tumor cells within the radiation field—cells that have evaded both chemotherapy and radiation. A strategy for improving long-terms outcomes for patients with LS-SCLC requires successful targeting of tumor cells destined to survive through standard therapy to inevitably give rise to recurrent disease (8). A better understanding of the mechanisms underlying chemoradiation (CRT) resistance is essential for the development of more effective and potentially curative strategies (9).

The molecular mechanisms responsible for rapidly emergent chemoresistant disease in SCLC have not been completely defined. One limitation for therapeutic development in SCLC has been the paucity of patient samples available at diagnosis and recurrence. Biopsies may only provide information on highly abundant molecules; processes critical to therapy-resistance and disease recurrence may be underrepresented prior to debulking. Patient-derived xenografts (PDXs) preserve most key genes, pathway activation, histology, and chemotherapy responsiveness of primary tumors (10–15). This *in vivo* platform has been useful for integrating drug screening with biomarker discovery in multiple tumor types (16–19). A key insight from studies of chemotherapy resistance in SCLC is that treatment resistance is most commonly associated with gene expression and epigenetic alterations, rather than acquired mutations (11). This finding has been consistently observed across independent PDX models and primary human tumor samples, suggesting that non-genomic mechanisms may play a major role in mediating therapeutic resistance in SCLC (11).

In this study, we modeled CRT resistance using SCLC PDXs and identified candidate resistance genes through transcriptomic profiling. Among these, Traf2- and Nck-interacting kinase (TNIK) was consistently upregulated in resistant tumors. *TNIK* has been implicated as a driver of tumorigenesis and therapy resistance in several cancers (20–31). TNIK inhibition with the small molecule inhibitor, NCB-0846, was shown to abrogate tumor growth in these studies (20,21,23–29). However, the role of TNIK in CRT resistance in SCLC has not been investigated yet. In this study, we utilized both *in vitro* and *in vivo* preclinical models to test whether TNIK inhibition can enhance the responsiveness of SCLC to CRT treatment. Our findings highlight that TNIK inhibition sensitizes SCLC xenograft tumors when combined with CRT and therefore, TNIK can be a potentially targetable oncogenic driver in LS-SCLC.

Materials and Methods

Cell Line and Reagents

Small cell lung cancer cell line H446 (RRID: CVCL_1562), H196 (RRID: CVCL_1509), H2196 (RRID: CVCL_1539), DMS114 (RRID: CVCL_1174) and H2286 (RRID: CVCL_1545) cells were purchased from the ATCC on 09.15.2024. H446, H196 and DMS114 are cultured in RPMI-1640 medium (Gibco; #11875119) supplemented with 10% fetal bovine serum (Gemini; #100-106) and 1% of penicillin/streptomycin (Gibco; #15140122). H2196 is cultured in HITES medium. HITES medium is DMEM:F12 medium (Gibco; #11320033) supplemented with 0.005 mg/ml Insulin (Sigma-Aldrich; #I9278), 0.01 mg/ml Transferrin (Sigma-Aldrich; #T8158), 30nM Sodium selenite (Sigma-Aldrich; #S5261), 10 nM Hydrocortisone (Sigma-Aldrich; #H0888), 10 nM beta-estradiol (Sigma-Aldrich; #E2758), extra 2mM L-glutamine (for final conc. of 4.5 mM) (Gibco; #25030081), 5% fetal bovine serum and 1% of penicillin/streptomycin. H2286 is cultured in RPMI-1640 medium supplemented with 5% fetal bovine serum and 1% of penicillin/streptomycin. All cell lines were cultured at 37℃ and 5% CO2 humidified incubator. Total cell counts were obtained using the T10 Automated cell counter system (Bio-Rad; #1450010). All cells were tested for Mycoplasma contamination and authenticated with short tandem repeat profiling by Translational Laboratory Shared Resources (TLSR) at UMB on 10.25.2024.

For *in vitro* uses, Cisplatin (MedChemExpress; HY 17394/CS-1122) was reconstituted daily in saline at 1 mM. Etoposide (MedChemExpress; HY-13629/CS-1774) was reconstituted in DMSO at 1 mM. TNIKi (NCB-0846; Selleck Chemicals; #S8392) was reconstituted in 100% ethanol at 5mM. For *in vivo* use, Cisplatin (Accord; #NDC 16729-288-11) and Etoposide (Accord; #NDC 16729-114-31) were purchased from the Johns Hopkins Hospital pharmacy. Cisplatin was diluted in saline and Etoposide was diluted in saline or PBS. TNIKi was prepared daily in 10% DMSO with 90% pharmaceutical grade corn oil (MedChemExpress; HY-Y1888/CS-004037).

SCLC xenograft models and treatment dosing

All *in vivo* experiments were performed in accordance with protocols approved by the Animal Care and Use Committee of the Johns Hopkins University (Baltimore, MD). The LX33 PDXs were isolated and passaged as previously described (12,32,33). LX47 PDXs were passaged as tumor tissue sections (~3 mm) coated in Matrigel and implanted via subcutaneous flap incisions. LU73, LU86, and LU148 PDXs were provided to us from Stemcentrx (now AbbVie, RRID: SCR_010484). LX33, LX47, LU73, LU86, and LU148 PDXs were derived from chemotherapy-naïve patients with SCLC. Resistance modeling in SCLC PDXs was previously demonstrated through treating SCLC PDX tumors and analyzing tissue at the point of maximal response (10). Transcriptional profiling elucidated an enrichment of discrete genes at maximal response time points. Gardner et al. (10) demonstrated mechanisms of chemotherapy resistance in chemotherapy-treated PDXs following 6-8 months of treatment. Based on our observation of differential gene expression as early as one week into therapy, we hypothesized that increasing the frequency of non-curative treatment would accelerate the development of a chemoradiotherapy-resistant PDX model. All *in vivo* experiments were performed in female NOD-SCID immunodeficient mice, 4 to 6 weeks old at the time of PDX/CDX implantation (JHU; NOD.Cg-Prkdc^{scid}/J). Once tumor volumes reached approximately 150-250 mm^3, mice

were randomly assigned into weekly treatment arms. For the initial CRT studies, mouse cohorts received: 1) vehicle control (PBS/Saline); 2) Cisplatin 5 mg/kg on day 1 (D1) plus Etoposide 8 mg/kg on days 1-3 (D1-3) (CT); 3) Radiotherapy (RT) 3 Gy x 1 weekly; or 4) CT plus RT (CRT). For the TNIK inhibitor studies, the mouse cohorts received 1) vehicle control (PBS/Saline); 2) CRT; 3) NCB-0846 only on days 1, 3 and 5 (D1, D3 and D5) by oral gavage or 4) CRT plus NCB-0846 100 mg/kg 3x/week by oral gavage weekly. Chemotherapy treatment consisted of pre-hydration (saline) of at least 1 hour before receiving Cisplatin (5 mg/kg) on d1, q1w and Etoposide (8mg/kg) d1-3, q1w, via oral gavage. Radiotherapy was facilitated with the use of the Johns Hopkins University Small Animal Radiation Research Platform (Xstrahl) (34,35). To validate our *in vitro* results with $TNIK^{high}$ SCLC cells, H446 ($1x10^6$ cells) were subcutaneously implanted into the flank of NOD-SCID mice in a 1:1 PBS:Matrigel mixture. For PDX tumors, treatment lasted for four weeks while for CDX tumors treatment lasted for about 2 weeks. Changes in tumor volumes were assessed 3-4 times a week through digital caliper measurements. Tumor volume was calculated using the formula: tumor volume = (length x $width^2$)/2. For statistical analysis, tumor volume was normalized to the baseline volume.

RNA isolation and genome-wide transcriptional profiling

Total RNA was isolated using the RNeasy mini kit (Qiagen, Hilden, Germany). Following RNA isolation, total RNA integrity was checked by the 2100 Bioanalyzer (Agilent Technologies, Santa Clara, CA). RNA concentrations were measured using the NanoDrop system (Thermo Fisher Scientific, Inc., Waltham, MA). Preparation of RNA sample library and sequencing were performed by the Genomics Core Laboratory at Weill Cornell Medicine. Using Illumina Stranded Total RNA Sample Library Preparation kit (Illumina, San Diego, CA), rRNAs and abundant globin mRNAs were depleted, and cDNA synthesis was completed, adapters were ligated, and unique dual indexes were added by PCR amplification according to the manufacturer's instructions. The final libraries were quantified and normalized prior to sequencing. The pooled cDNA libraries were sequenced on Illumina NovaSeq 6000 sequencer with pair-end 100 cycles. The raw sequencing reads in BCL format were processed through bcl2fastq 2.19 (Illumina) for FASTQ conversion and demultiplexing. Raw gene expression data have been deposited in Zenodo and are permanently available at the following URL: https://doi.org/10.5281/zenodo.18260211.

Preprocessing and quantification

Quality checks and preprocessing were performed to ensure the quality of the libraries. Transcript expression quantification was performed using salmon (v1.3.0) (36) and Ensembl 104 transcript models. Tximport R/Bioconductor package (37) was used to summarize transcript counts to gene level and to perform length-scaled transcript per million normalizations.

Differential gene expression analysis

Differential gene expression analysis was performed with trimmed mean of M-values (TMM) normalized expression values (38) and fitting a generalized linear model (GLM) approach coupled with empirical Bayes moderation of standard errors and voom precision weights (39,40). The p-values were adjusted to control for multiple hypothesis testing using the Benjamini-Hochberg method and genes with false discovery rate (FDR) equal or less than 0.05 were reported. Each treatment arm was compared to its respective control group within each PDX. For the meta-analysis of all PDXs the standardized mean differences were estimated by Hedge's g

method (41) and the between study variance was estimated by restricted maximum likelihood using the *meta* R package.

Gene set enrichment analysis

For the gene set enrichment analysis we applied a non-competitive rotation approach (42) implemented in the limma package (RRID: SCR_010943) (39). Briefly, the gene expression and design matrices used in the differential gene expression analysis were used as input to the *fry* function. The gene set statistic was set to 'mean'. Wikipathways gene sets were obtained from the Broad Institute MSigDB database. Gene sets with a FDR equal or less than 0.1 on directional tests were considered significant.

Cell viability assay

Cisplatin (MedChemExpress; HY 17394/CS-1122) and Etoposide (MedChemExpress; HY-13629/CS-1774) solutions were prepared in 0.9% saline and DMSO, respectively. NCB-0846 solutions (Selleck Chemicals; #S8392) were prepared in 100% ethanol. Cells were seeded in triplicates at 2,000-5,000 cells/well in 96-well white microplates (Corning; #3603). 24h later, working solutions of drugs or vehicle controls were added at a 1:100 dilution. Cells were cultured for another 48h or 72h. The CellTiter-Glo 2.0 assay (Promega; #G9242) was used to assess cell viability according to the manufacturer's protocol.

Assessment of drug synergy

Cells were seeded in duplicates in 96-well white microplates. 24h later, cells were treated with vehicles, single-agent drugs, or various combinations of NCB-0846 with cisplatin/etoposide. Drug concentrations were selected as recommended by the Chou-Talalay method (43). Drug synergy data were obtained using the CellTiter-Glo 2.0 assay and analyzed with the Zero Interaction Potency (ZIP), Bliss, Loewe, and Highest Single Agent (HSA) models using the SynergyFinder 2.0 web tool (RRID: SCR_019318) (44–46). A synergy score higher than 10 indicates synergism, a score lower than -10 antagonism, and a score in between additivity.

Cell irradiation and clonogenic assays

Cells were seeded onto 6-well plates at $1x10^5$-$2x10^5$ cells per well. After treatment with vehicle, single-agent NCB-0846, cisplatin, etoposide or drug combinations for 24 or 48h, old culture media was replaced with fresh media. In case of TNIK siRNA conditions, cells were transfected with siTNIK or scramble control at day 1, followed by media change on day 2. Cells were then given 2, 4, or 6 Gy of ionizing radiation with the X-Rad 320 Biological Irradiator (Precision X-Ray Inc.) or the CIXD X-Ray Irradiator (X-Strahl). 24h after irradiation, cells were trypsinized and counted for plating onto 60-mm dishes. Cells irradiated with 0, 2, 4, and 6 Gy were seeded in duplicates at 8000, 16000, 64000 and 128000 cells per dish, respectively. Cells were incubated until the emergence of colonies with over 50 cells, which took 7-21 days. Culture media was replenished weekly. Colonies were fixed with 20% methanol and stained with 0.5% crystal violet and counted for survival fraction analysis as previously described (47,48).

Immunoblotting

Protein from cultured cells and xenograft tumors was harvested, resolved with gel electrophoresis, and transferred to PVDF membranes as previously described (48). After a blocking step for 1h at room temperature, membranes were incubated with primary antibodies

overnight at 4°C. Blots were then washed with tris-buffered saline (TBS) with 0.1% Tween-20 before incubation with horseradish peroxidase (HRP)-conjugated secondary antibodies for 1h at room temperature. Protein expression was visualized using enhanced chemiluminescence detection with the Amersham ECL kit (Cytiva; #RPN2106) and using the Chemidoc Imaging system (Biorad). Primary antibodies include Chk1 (Cell Signaling Technology Cat# 2360S, RRID: AB_2080320), p-Chk1 (S345) (Cell Signaling Technology Cat# 2348S, RRID: AB_331212), Chk2 (Cell Signaling Technology Cat# 2662S, RRID: AB_2080793), p-Chk2 (T68) (Cell Signaling Technology Cat# 2661S, RRID: AB_331479), ATM (Cell Signaling Technology Cat# 2873S, RRID: AB_2062659), p-ATM (S1981) (Cell Signaling Technology Cat# 5883S, RRID: AB_10835213), ATR (Cell Signaling Technology Cat# 13934S, RRID: AB_2798347), p-ATR (S428) (Cell Signaling Technology Cat# 2853S, RRID: AB_2290281), p-histone H2AX (S139) (Cell Signaling Technology Cat# 9718, RRID: AB_2118009), p-histone H3 (S10) (Cell Signaling Technology Cat# 9701S, RRID: AB_331535), histone H3 (Cell Signaling Technology Cat# 4499S, RRID: AB_10544537), cGAS (Cell Signaling Technology Cat# 15102S, RRID: AB_2732795), p-STING (S366) (Cell Signaling Technology Cat# 50907S, RRID: AB_2827656), STING (Cell Signaling Technology Cat# 13647S, RRID: AB_2732796), β-actin (Cell Signaling Technology Cat# 4970S, RRID: AB_2223172), vinculin (Cell Signaling Technology Cat# 13901S, RRID: AB_2728768). Secondary antibodies include anti-mouse IgG HRP-linked (Cell Signaling Technology Cat# 7076, RRID: AB_330924) and anti-rabbit IgG HRP-linked (Cell Signaling Technology Cat# 7074, RRID: AB_2099233).

Immunohistochemistry

Immunostaining was performed at the Oncology Tissue Services Core of Johns Hopkins University School of Medicine. Immunolabeling for ASCL1/MASH1 and NeuroD1 was performed on formalin-fixed, paraffin-embedded sections on a Ventana Discovery Ultra autostainer (Roche Diagnostics). Briefly, following dewaxing and rehydration on board, epitope retrieval was performed using Ventana Ultra CC1 buffer (catalog# 6414575001, Roche Diagnostics) at 96^{o}C for 64 minutes. Primary antibodies anti-MASH1(Abcam Cat# ab211327, RRID: AB_2924270) and anti-NeuD1 (Abcam Cat# ab205300, RRID: AB_3083561) was applied at 36^{o}C for 60 minutes. Primary antibodies were detected using an anti-rabbit HQ detection system (catalog# 7017936001 and 7017812001, Roche Diagnostics) or anti-mouse HQ detection system (catalog# 7017936001 and 7017782001, Roche Diagnostics) as applicable followed by Chromomap DAB immunohistochemistry (IHC) detection kit (catalog # 5266645001, Roche Diagnostics), counterstaining with Mayer's hematoxylin, dehydration and mounting.

Cell cycle profiling assay

Cells were seeded onto 6-well plates with $2x10^5$ to $3x10^5$ per well and treated with either vehicle or 300 nmol/L of NCB-0846. Cells were then incubated for another 48 hours, followed by 6Gy of IR. 24 hours after IR, cells were collected and fixed with 66% ice-cold ethanol and processed according to the manufacturer's protocol for Propidium Iodine Flow cytometry kit (Abcam; #ab139418). To finish, samples were analyzed with the BC Canto II (BD Biosciences) flow cytometer.

Evaluation of mitotic catastrophe by fluorescence microscopy

Cells were counted and seeded ($1.5x10^4$ per well) on sterilized, coverslips in 12-well plates on day 1. For H446 cells, Matrigel-coated coverslips were used. On day 1, coverslips in 12-well plates were incubated with 1mL coating media for 1 hour at room temperature, washed with PBS once and then with media before seeding cells. On day 2, cells were treated with vehicle or 300 nM NCB-0846, followed by media change and irradiation at 6 Gy on day 4. On day 5, cells were treated with 0.1 µg/mL colcemid (Gibco; #15212012) for 3 hours to enrich for mitotic cells. After 3 hours, cells were fixed with 4% PFA, washed with PBS, and stained with DAPI. Image acquisition was conducted with the Echo Revolution microscope at 40X magnification. Cells with multi-nucleated morphologies were determined to have undergone mitotic catastrophe (49)(50). Cells with micronuclei were assessed as previously described (48). A minimum of 25 fields of view and 500 cells were captured per sample for analysis.

siRNA transfection

The siRNA (TNIK siRNAs: Horizon Discovery, ON-TARGETplus SMART pool Human TNIK, Cat #L-004542-00-0010; Non-Targeting control siRNA: Horizon Discovery, ON-TARGETplus Control Pool Non-Targeting pool, #D-001810-10-05). Experiments were performed as described previously using Lipofectamine^{TM}3000 (Invitrogen, ThermoFisher Scientific) protocol (51). Briefly, cells were seeded on day 1, transfected on day 2 when they were 70% confluent, followed by media change and radiation (0, 2, 4, 6 Gy) on day 3.

Lentiviral transduction

To generate stable TNIK-overexpressing and mCherry-overexpressing cell lines, we purchased the following lentiviral particles from VectorBuilder (Chicago, Illinois): pLV[Exp]-EGFP:T2A:Puro-CMV>hTNIK[NM_015028.4] (VB220427-1219aqr) and pLV[Exp]-EGFP:T2A:Puro-EF1A>mCherry (VB010000-9298rtf). DMS114 cells were plated at $3x10^5$ cells per well in a 6-well plate. 24h later, cells were exposed to lentiviral particles prepared in culture media supplemented with 5 µg/mL polybrene (EMD Millipore; #TR-1003-G) for 16h. After a recovery period, puromycin selection (1 µg/mL) (Sigma-Aldrich; #P8833) and fluorescence-activated cell sorting were conducted to select for successfully transduced cells.

Alkaline comet assay

Human SCLC cells were treated with vehicle or 300 nM NCB-0846 for 48h, followed by media change and irradiation at 6 Gy or 10 Gy. 24h following IR treatment, cells were harvested and processed with the Alkaline CometAssay Single Cell Gel Electrophoresis Assay kit (BioTechne; #4250-050-K). Briefly, cells suspended in ice-cold 1X PBS at $5x10^5$ cells/mL were combined with molten LMAgarose at a 1:10 volume/volume ratio and spread onto CometSlides. Cells were lysed for 4 hours at 4°C and incubated with the Alkaline Unwinding Solution for 20 minutes at room temperature. Electrophoresis was conducted at 21 V for 30 minutes at 4°C. Slides were then washed with deionized water, 70% ethanol, and stained with 1X SYBR Gold (prepared in DMSO; Invitrogen; #S11494) for 30 minutes at room temperature. Images were captured at 100X magnification using the Revolution microscope (Echo). A minimum of 25 fields of view and 50 cells were imaged per replicate. Comet tail moment was calculated using the OpenComet 3.0 software.

Study Approval

All *in vivo* experiments were realized in accordance with the JHU IACUC approved protocols MO16M274, MO19M354 and MO22M320. Mice were housed in a pathogen-free environment

(animal facility of JHU Sidney Kimmel Comprehensive Cancer Center, Cancer Research Building).

Statistical analysis

All *in vitro* experiments were done with at least three independent biological replicates. For *in vivo* studies, tumor growth delay was determined using Kaplan-Meier estimate. Data were analyzed using either one-way Anova or two-way Anova with Tukey's post hoc HSD. All statistical analyses and graphs were carried out by using GraphPad Prism 10.0 (GraphPad Prism, RRID: SCR_002798).

Data Availability statement:

The data generated in this study are available upon request from the corresponding author.

Results

PDXs can be used to model and identify targets to combat rapid CRT resistance for LS-SCLC

To find candidate genes associated with CRT resistance, we evaluated transcriptional changes in a therapy-naïve SCLC PDX (LX33) in response to chemotherapy only (CT) and radiotherapy only, (RT) and combination treatment (chemoradiation, CRT). We treated LX33 PDX tumor-bearing mice with: 1) vehicle (control); 2) Cisplatin 5 mg/kg on D1 plus Etoposide 8 mg/kg on D1-3 (CT); 3) Radiotherapy 3 Gy x 1 on D1 (RT); and 4) CRT (**Fig 1A)**. We observed the greatest reduction in tumor size with the combination arm as compared to vehicle or single therapy arms (**Fig 1B and Supplementary Table 1**). Next, we performed whole transcriptome profiling between three biological replicates from all analyzed groups, collecting vehicle samples at D6, and treatment arms samples at D12 (**Fig 1B**). After pre-processing and normalization, we applied a generalized linear model approach coupled with empirical Bayes moderation of standard errors, identifying genes significantly associated with each treatment compared to control, as well as those changing differently upon CRT compared to single treatment modalities and represented as the UpSet plot (**Fig 1C**). Our results indicate that the CRT treatment arm has the most number of differentially expressed genes compared to the single therapy arms (**Fig 1C)**. This made us hypothesize that the genes modulated by CRT in LX33 PDX could be responsible for treatment resistance, and we compared our gene results to two previous genomic landscape studies (52,53). We found that *TNIK* and *HTR3C* were each upregulated in LX33 PDX exposed to CRT compared to single modality treatments, which also show CN gains in Rudin and George datasets (**Fig 1D**). *HTR3C,* which encodes for a serotonin receptor, is also interesting in light of previous work showing that inhibition of neuroactive ligand-receptor interactions with tricyclic antidepressants (TCAs) induces apoptosis in both chemonaïve and chemoresistant SCLC cells in culture, in mice and human SCLC tumors (54,55). However, inhibition of HTR3C (using citalopram) in the LX33 PDX model showed no anti-tumor benefits *in vivo* compared to CRT alone **(Supplementary Fig S1)**. Therefore, for the remainder of this study, we pursued TNIK as our primary target CRT resistance candidate.

***TNIK* is a chemoradiation resistance candidate gene in multiple SCLC PDX models**

To recapitulate the tumor heterogeneity found in SCLC patients, we characterized the treatment response of a panel of 4 additional therapy-naïve PDXs (LU86, LU148, LX47, and LU73) to

single therapy (RT or CT only) and combination (CRT) as shown in the schematic workflow (**Fig 2A)**. Our panel of PDXs encompasses both classic (SCLC-A) and variant (SCLC-N) subtypes as shown by IHC (**Fig 2B**). We found that neither SCLC-A nor SCLC-N PDXs was associated with better RT or CT responses. All the PDXs (LU86, LU148, LX47, and LU73), however, were highly sensitive to CRT treatment as shown by final tumor volumes that were smaller by > 50% at the end of the treatment regimens (**Fig 2C and Supplementary Tables 2-6**). LX33 displayed the least pronounced response to CRT. Despite significant reduction in tumor volume by combination treatment in LX33 PDX compared to the single therapy arms, the tumor continued to grow (**Fig 2C and Supplementary Table 2**). All the PDXs analyzed exhibited a diverse profile of response to each of the treatment arms, supporting that the PDXs used in this study reflect the heterogeneity expected across SCLC patients. Furthermore, none of the treatments were able to cause complete tumor regression. Since CRT treatment is the backbone of SOC for LS-SCLC, we focused on this treatment tumor response as a model to profile the molecular features of the remaining resistant tumor cells that survived throughout the treatment.

We performed RNA-sequencing of the 5 PDXs across two different timepoints: i) the second week after the first treatment round (also labeled "early"); and ii) at the end of the treatment regimen (labeled "late") for each arm. Principal component analysis (PCA) (**Fig 2D**) could easily discriminate each PDX model in our study confirming that these models represent a heterogenous group. Moreover, we observed that the expression profiles for each treatment arm for individual PDXs were remarkably similar to each other. This suggests that the transcriptional differences between naïve and resistant cells were more subtle at the transcriptional level.

At the end of the CRT treatment, none of the PDXs demonstrated complete remission of the tumors, suggesting the remaining tumor cells after CRT treatment were resistant. We performed a meta-analysis of all PDXs to identify genes associated with CRT resistance. To this end, we compared CRT at final treatment to their respective control arms. We found 57 genes differently expressed in the CRT-resistant sub-population of tumor cells (|Hedge's g| >= 0.5 and p-value <= 0.01). Among the top up-regulated genes were *COLCA1*, *ABCG1*, *GPR155*, *ATP2A1*, and *TNIK*, while top down-regulated genes included *H2AC6*, *UBR7*, *SNORD3A*, *CDH2*, and *SEPTIN3* (**Fig 2E**). When compared to our original list derived from LX33 alone (**Fig 1D**), we found that only *TNIK* remained at the intersection. Interestingly, we found that higher *TNIK* expression correlated with smaller tumor volume across all the PDXs suggesting that TNIK is enriched in surviving resistant cells (**Supplementary Fig S2)**. Moreover, of the top differentially expressed genes, only *TNIK* was found recurrently amplified in human SCLC tumor samples (52,53).

When each PDX was analyzed individually, we found that only one gene, *TNIK*, was consistently differentially expressed (adjusted P-value ≤ 0.1) across all PDXs at the end of the CRT treatment. TNIK expression was elevated at the conclusion of the treatment cycles for every PDX (**Fig. 2F and Supplementary Fig. S3A**). This pattern suggests that TNIK upregulation is not merely a direct consequence of the CRT response, but rather an inherent feature of resistant cells. We also observed that Wnt signaling—a pathway linked to TNIK—was upregulated in 4 of the 5 PDXs treated with CRT (**Supplementary Fig. S3B**). These findings suggest that TNIK expression may be associated with a tumor subpopulation that is resistant to CRT.

TNIK inhibition sensitizes TNIK^{high} SCLC cells to CRT

We explored whether TNIK inhibition could enhance CRT sensitivity of SCLC cells. To inhibit TNIK, we used NCB-0846 (TNIKi), which traps TNIK in an inactive conformation (21). We employed a panel of human SCLC cell lines with low (DMS114 and H2286) or high (H446, H196 and H2196) TNIK expression (**Fig 3A)**. While short-term cell viability showed that $TNIK^{low}$ SCLC cells had similar sensitivity to TNIKi as $TNIK^{high}$ SCLC cells, long-term cell viability showed that $TNIK^{high}$ H446 cells are more sensitive to TNIKi compared to $TNIK^{low}$ DMS114 cells (**Fig 3B and Supplementary Fig S4)**. After determining the response of these cell lines to pharmacologic TNIKi and chemotherapy drugs (cisplatin and etoposide), drug synergy assays were conducted to assess the interaction between TNIKi and chemotherapy (**Supplementary Fig S5A)**. We mostly observed additive interactions between TNIKi and chemotherapy at 48-72hrs post treatment for all SCLC cell lines tested (**Supplementary Fig S5B)**.

We then investigated whether TNIK inhibition could sensitize to ionizing radiation (IR) by comparing the long-term survival of SCLC cells treated with TNIKi vs. vehicle before exposure to IR. Pre-treatment with TNIKi over a 24h or 48hrs period reduced the survival of $TNIK^{high}$ H446 cells at all tested IR doses (0-6 Gy) , suggesting that TNIKi may radiosensitize $TNIK^{high}$ SCLC cells (**Fig 3C)**. In contrast, TNIKi failed to sensitize $TNIK^{low}$ DMS114 cells to radiation, suggesting that the radiosensitization effect of TNIK inhibitor depends on TNIK expression and cellular context (**Fig 3C**).

We then used *TNIK* siRNA or scramble control to knockdown *TNIK* in $TNIK^{high}$ H446 cells, followed by their exposure to IR (0-6 Gy). Similar to pharmacological TNIKi, genetic knockdown of TNIK sensitized $TNIK^{high}$ SCLC cells to radiation (**Fig 3D).** These results suggest that TNIK is required for favorable radiation resistance *in vitro* for $TNIK^{high}$ SCLC cells. Furthermore, we stably overexpressed TNIK or mCherry (control) in $TNIK^{low}$ DMS114 cells, followed by exposing these cells to IR (**Fig 3E**). TNIK overexpression dramatically enhanced survival in response to IR in DMS114 cells (**Fig 3E**), highlighting that TNIK is also sufficient for radiation resistance in SCLC cells *in vitro*.

Finally, to assess the interactions between TNIKi and CRT, we evaluated the post-IR survival of cells treated with single-agent TNIKi, cisplatin, or both. We found that TNIKi in combination with cisplatin is the most effective in sensitizing $TNIK^{high}$ SCLC cells to radiation at all the tested doses. However, this effect is not observed in $TNIK^{low}$ SCLC cells (**Supplementary Fig S6)**. Collectively, these results suggest that TNIKi can sensitize $TNIK^{high}$ SCLC cells to CRT.

TNIK inhibition impairs the DNA damage response in $TNIK^{high}$ SCLC cells exposed to radiation

To elucidate the mechanisms whereby TNIK inhibition may increase radiosensitivity, we explored the impact of TNIKi on the DNA damage response (DDR) signaling. To evaluate how TNIKi impacted the DDR in response to IR, we treated $TNIK^{high}$ cells with TNIKi or vehicle with and without radiation. We probed the activation status of DDR proteins over time in $TNIK^{high}$ cells pretreated with TNIKi or vehicle before IR. γH2AX is a DNA breaks marker, and combining TNIKi treatment with radiation in $TNIK^{high}$ H446 cells led to a higher level of γH2AX than radiation alone at both 1hr and 24 hr (**Fig 4A**). Next, we looked at the DDR pathway that may be impaired by TNIKi. When examining ATM-CHK2 and ATR-CHK1 DDR signaling we observed a prolonged activation of phospho-CHK2 (p-CHK2) in $TNIK^{high}$ cells treated with TNIKi plus radiation compared to only radiation at both timepoints (**Fig 4A)**. We did not observe

any difference in CHK1 levels between TNIKi plus radiation versus radiation alone (**Fig 4A**). This is consistent with previous findings that TNIKi does not disrupt the ATR-CHK1 DDR pathway (20). Importantly, the TNIKi did not affect the post-IR DDR in TNIK^{low} cells, supporting that TNIKi-mediated radiosensitization is dependent on TNIK (**Fig 4A**). Direct evaluation of DNA damage with the alkaline comet assay, which detects both single-strand breaks (SSBs) and double-strand breaks (DSBs), confirmed that TNIKi treatment with radiation in TNIK^{high} H446 cells led to a higher level of DNA damage than radiation alone (**Fig 4B**). Interestingly, TNIK overexpression increased the DNA damage repair in TNIK^{low} DMS114 cells post radiation at both 1hr and 24 hr (**Supplementary Fig S7)**. TNIK-overexpressing DMS114 cells had a lower level of γH2AX at both timepoints compared to control mCherry-overexpressing cells, post radiation (**Supplementary Fig S7)**. These results suggest that TNIK is sufficient for radioresistance in SCLC cells.

TNIK inhibition disrupts radiation-induced cell cycle arrest and promotes mitotic catastrophe

Radiation-induced DNA damage normally results in cell cycle arrest, so we next explored the impact of TNIKi on the cell cycle of both TNIK^{high} and TNIK^{low} SCLC cells following treatment with IR (**Fig 4C and Supplementary Fig S8)**. Following IR, most SCLC cells are arrested at G2. TNIKi pretreatment decreased the relative G2 population, indicating bypass of the G2/M checkpoint and allowing cells to resume cell division (**Fig 4C and Supplementary Table 7)**. Notably, TNIKi treatment along with radiation increased the percentage of cells in the sub-G1 fraction, indicating more apoptotic cells (**Fig 4C and Supplementary Table 7**). However, we observed a similar phenotype in TNIK^{low} cells, (**Fig 4C and Supplementary Table 7)** and this could be due to the off-target effects of the inhibitor (21). Analysis of phospho-histone H3 (pH3) revealed that, following radiation, TNIK inhibition increases cell cycle progression and mitosis in TNIK^{high} H446 cells (**Supplementary Fig S8A)**, while TNIK overexpression has the opposite effect in TNIK^{low} DMS114 cells (**Supplementary Fig S8B)**. These results suggest that TNIK modulates cell cycle response in SCLC cells post radiation.

The consequences of cell cycle progression with DNA damage may lead to mitotic catastrophe and apoptosis. We visualized mitotic catastrophe in the irradiated cells with and without TNIKi treatment by observing the nuclear morphology of cells post-IR (**Fig 4D)**. Cells undergoing mitotic catastrophe had a fragmented nucleolus and micronuclei formation. We observed that TNIK inhibition combined with radiation induced more mitotic catastrophe in TNIK^{high} H446 cells compared to radiation alone (**Fig 4D and Supplementary Fig S9A)**. We did not observe this effect in TNIK^{low} cells (**Fig 4D)**. Interestingly, TNIK overexpression in TNIK^{low} DMS114 cells reduced mitotic catastrophe post radiation, confirming that TNIK is involved in regulating mitotic catastrophe in SCLC cells with DNA damage (**Supplementary Fig S9B)**.

Inhibition of TNIK promotes CRT sensitivity in SCLC xenograft tumors

We validated TNIK as a druggable CRT resistance target *in vivo* using a therapy naïve PDX (LX33) and TNIK^{high} SCLC cells H446. Tumor moribund mice were randomized to the following weekly treatment arms: 1) vehicle control (n=6); 2) Cisplatin 5 mg/kg on D1 plus Etoposide 8 mg/kg on D1-3 plus Radiotherapy 3 Gy x 1 (CRT) weekly (n=8); 3) NCB-0846 (TNIKi) only (n=7) and 4) CRT plus TNIKi 100 mg/kg 3x/week (n=8) by oral gavage weekly (**Fig 5A)**. Differential TNIK overexpression was preserved in the xenograft tumors (**Fig 5B).** We

observed a major reduction in tumor volume in the CRT treatment group vs control or TNIKi alone treatment groups. Remarkably, the inclusion of the TNIKi with CRT further delayed tumor growth in both LX33 PDX and H446 CDX tumors (**Fig 5C**). These results demonstrate that TNIK plays a role in conferring resistance to CRT therapy in a therapy-naïve SCLC PDX and CDX, and TNIKi in combination with CRT is most effective in delaying tumor growth of SCLC tumors. Additionally, the treatment regimens were well tolerated as determined by the weight of the mice over the treatment regimens (**Fig 5D).**

Discussion

Concurrent CRT followed by consolidation with the anti-PDL-1 antibody, durvalumab, is the standard first line treatment for LS-SCLC and affords > 30% 5-year OS. However, the majority of LS-SCLC patients who receive SOC therapy still develop recurrent disease which is often treatment refractory. While consolidation with durvalumab reduces the risk of extrathoracic relapse, it does not decrease the incidence of local (in-field) recurrence. The mechanisms driving resistance to chemoradiation remain poorly understood but are critical to improving outcomes in LS-SCLC. To identify molecular targets to improve CRT outcomes in LS-SCLC, we used the LX33 PDX to study acute gene expression changes that may be associated with emerging resistance. When treated with CRT, we observed a major response in the LX33 PDX compared to vehicle or single treatment arms. This was further confirmed by whole transcriptome RNA-profiling, which identified genes significantly upregulated and downregulated in the CRT arm compared to control or single therapy, indicating that these genes could be involved in SCLC treatment resistance in patients. When we compared our results to previous studies, we found the *TNIK* gene to be consistently upregulated and also showed copy number gains in human genomic studies.

Our study in total included 5 therapy-naïve PDXs, and we consistently found the population of CRT-resistant SCLC cells exhibited increased *TNIK* expression. Furthermore, none of the PDXs displayed complete tumor remission at the end of the CRT treatment, raising the possibility of *TNIK* playing a role in treatment resistance. *TNIK* was also frequently amplified in SCLC patient samples. We confirmed TNIK as a candidate *in vivo*, treating with CRT plus the small molecule inhibitor of TNIK (NCB-0846) and observed a tumor response (reduction in tumor size in the case of H446 CDX tumors) in the combination arm compared to control and CRT only arms.

Previous studies suggest that TNIK regulates multiple signaling pathways that might promote CRT resistance (22–31). From our lab, we have shown that TNIK plays a role in CRT resistance in lung squamous cell carcinoma (LSCC) (20), which shows frequent *TNIK* amplification (25), and demonstrated that TNIK inhibition sensitized $TNIK^{high}$ LSCC to radiation therapy (20). Given these data in LSCC, we explored whether TNIK inhibition could enhance the vulnerability of SCLC cell lines to CRT and found that the inhibitor NCB-0846 also sensitized $TNIK^{high}$ H446 cells to radiotherapy, possibly via impairing the DNA damage response in those cells, while it failed to radiosensitize $TNIK^{high}$ H2196 cells, suggesting that TNIK inhibitor-mediated radiosensitization in SCLC is cell-line dependent. The compound NCB-0846 is a well-characterized small molecule inhibitor of TNIK (21,26–28), which traps the protein in an inactive conformation and impedes the kinase activity of TNIK (21). We also validated TNIK as a radiation resistance target genetically by siRNA knockdown in $TNIK^{high}$ SCLC cells and found that, similar to pharmacological inhibition, genetic inhibition also sensitized SCLC cells to radiation, suggesting that TNIK is a requirement for radioresistance in $TNIK^{high}$ SCLC cells *in vitro*. Furthermore, when we overexpressed TNIK in $TNIK^{low}$ SCLC cells, followed by exposure to radiation, the cells became more resistant to radiotherapy, highlighting that TNIK expression is sufficient to cause radiation resistance *in vitro* in SCLC cells. To validate our *in vitro* results, we treated a $TNIK^{high}$ (H446) xenograft tumor with the inhibitor NCB-0846 plus CRT, and the combination treatment was the most effective at inhibiting xenograft tumor growth. These collective findings support our hypothesis that TNIK plays a direct role in SCLC treatment resistance and that TNIK inhibition can sensitize SCLC tumors to CRT.

Limitations of our study encompass those that pertain to xenograft and PDX models, which include the lack of an immune microenvironment which plays a role in shaping tumor responses to CRT treatment. Furthermore, even though we included 5 different PDX models, the lack of genetic heterogeneity in our models limits the assessment of the combination treatment on heterogeneous tumors that represent SCLC patients. Therefore, it will be important to validate TNIKi as a radiosensitizing strategy in models that better capture SCLC biology, such as genetically engineered mouse models. Another limitation is the specificity of the inhibitor NCB-0846 targeting other kinases besides TNIK, such as FLT3, JAK3, PDGFRα, TRKA, CDK2/CycA2 and HGK (21). Surprisingly, we observed some effects of the inhibitor on cell cycle in $TNIK^{low}$ cells, and therefore, our data suggests that NCB-0846 disrupts the G2/M cell cycle checkpoint in SCLC cells independent of their TNIK expression.

Phospho-histone H3 analysis confirmed that TNIK regulates the cell cycle responses in SCLC cells following radiation. Our study also confirmed that TNIK is involved in regulating mitotic catastrophe in SCLC cells with DNA damage. Mechanistically, TNIK inhibition compromises DNA damage repair, thereby sensitizing SCLC cells to radiotherapy by promoting mitotic catastrophe.

In conclusion, our findings highlight the potential of TNIK as a promising therapeutic target in LS-SCLC to combat CRT resistance. We have shown that by coupling TNIKi with CRT *in vivo*, we are not only able to eradicate SCLC tumors but also increase their sensitivity to CRT treatment. Since PDXs preserve the treatment responsiveness of primary tumors and the TNIKi is well tolerated in our *in vivo* studies, investigating TNIKi strategies in the clinic as a treatment option is warranted for LS-SCLC.

Acknowledgments: We would like to acknowledge support from the Animal facility, Small Animal Radiation Research Platform (SARRP), and Oncology Tissue Services (OTS) core facilities at the Johns Hopkins School of Medicine and the Flow Cytometry, Experimental irradiator and Division of Translational Radiation Sciences (DTRS) core facilities at the University of Maryland School of Medicine.

Financial support: This work was supported by the National Cancer Institute (NCI) (U01CA231776). CLH was funded by the NIH/NCI U01CA231776 and the Cigarette Restitution Fund (CRF). PTT was funded by the Movember Foundation-Distinguished Gentlemen's Ride-Prostate Cancer Foundation Challenge Award (20CHAL03), the NIH/NCI (U01CA212007, U01CA231776, 1R01CA271540 and U54CA273956), the Department of Defense (W81XWH-21-1-0296) and by an anonymous donor.

Author contributions: DDC, EI and **NC** equally and successively participated in performing the experiments, and in acquiring and analyzing data under the direction of **PTT, LM** and **CLH**. **JC**, **AC, WHT, AL**, **FAC**, **TN**, **DNW**, **ES**, **ACS**, **YS**, **MAK**, and **MR** performed animal husbandry, and/or provided technical assistance with the bulk of the experiments, and/or participated to data processing and analyses, and/or provided reagents, and/or provided pathology analyses and scoring, and/or provided critical intellectual contributions, and/or participated in reviewing the manuscript. **DDC, EI, NC**, **PTT, CLH and LM** designed the research project, acquired, analyzed, and interpreted the data, provided critical intellectual contributions, and wrote, prepared, and submitted the manuscript for publication.

References

1. Torres-Durán M, Curiel-García MT, Ruano-Ravina A, Provencio M, Parente-Lamelas I, Hernández-Hernández J, et al. Small-cell lung cancer in never-smokers. ESMO Open. 2021;6:100059.

2. Wang Q, Gümüş ZH, Colarossi C, Memeo L, Wang X, Kong CY, et al. SCLC: Epidemiology, Risk Factors, Genetic Susceptibility, Molecular Pathology, Screening, and Early Detection. J Thorac Oncol. 2023;18:31–46.

3. Siegel RL, Kratzer TB, Giaquinto AN, Sung H, Jemal A. Cancer statistics, 2025. CA Cancer J Clin. 2025;75:10–45.

4. Kalemkerian GP, Schneider BJ. Advances in Small Cell Lung Cancer. Hematol Oncol Clin North Am. 2017;31:143–56.

5. Senan S, Okamoto I, Lee G-W, Chen Y, Niho S, Mak G, et al. Design and Rationale for a Phase III, Randomized, Placebo-controlled Trial of Durvalumab With or Without Tremelimumab After Concurrent Chemoradiotherapy for Patients With Limited-stage Small-cell Lung Cancer: The ADRIATIC Study. Clin Lung Cancer. 2020;21:e84–8.

6. Cheng Y, Spigel DR, Cho BC, Laktionov KK, Fang J, Chen Y, et al. Durvalumab after Chemoradiotherapy in Limited-Stage Small-Cell Lung Cancer. N Engl J Med. 2024;391:1313–27.

7. Senan S, Cheng Y, Spigel DR, Cho BC, Laktionov K, Zenke Y, et al. 297MO: Patterns of disease progression with durvalumab (D) after concurrent chemoradiotherapy (cCRT) in limited-stage small-cell lung cancer (LS-SCLC): Results from ADRIATIC. Journal of Thoracic Oncology. Elsevier; 2025;20:S181–2.

8. Pietanza MC, Byers LA, Minna JD, Rudin CM. Small cell lung cancer: will recent progress lead to improved outcomes? Clin Cancer Res. 2015;21:2244–55.

9. Bunn PA, Minna JD, Augustyn A, Gazdar AF, Ouadah Y, Krasnow MA, et al. Small Cell Lung Cancer: Can Recent Advances in Biology and Molecular Biology Be Translated into Improved Outcomes? J Thorac Oncol. 2016;11:453–74.

10. Gardner EE, Connis N, Poirier JT, Cope L, Dobromilskaya I, Gallia GL, et al. Rapamycin rescues ABT-737 efficacy in small cell lung cancer. Cancer Res. 2014;74:2846–56.

11. Gardner EE, Lok BH, Schneeberger VE, Desmeules P, Miles LA, Arnold PK, et al. Chemosensitive Relapse in Small Cell Lung Cancer Proceeds through an EZH2-SLFN11 Axis. Cancer Cell. 2017;31:286–99.

12. Daniel VC, Marchionni L, Hierman JS, Rhodes JT, Devereux WL, Rudin CM, et al. A primary xenograft model of small-cell lung cancer reveals irreversible changes in gene expression imposed by culture in vitro. Cancer Res. 2009;69:3364–73.

13. Fichtner I, Rolff J, Soong R, Hoffmann J, Hammer S, Sommer A, et al. Establishment of patient-derived non-small cell lung cancer xenografts as models for the identification of predictive biomarkers. Clin Cancer Res. 2008;14:6456–68.

14. Tentler JJ, Bradshaw-Pierce EL, Serkova NJ, Hasebroock KM, Pitts TM, Diamond JR, et al. Assessment of the in vivo antitumor effects of ENMD-2076, a novel multitargeted kinase inhibitor, against primary and cell line-derived human colorectal cancer xenograft models. Clin Cancer Res. 2010;16:2989–98.

15. Rubio-Viqueira B, Hidalgo M. Direct in vivo xenograft tumor model for predicting chemotherapeutic drug response in cancer patients. Clin Pharmacol Ther. 2009;85:217–21.

16. Rajeshkumar NV, Tan AC, De Oliveira E, Womack C, Wombwell H, Morgan S, et al. Antitumor effects and biomarkers of activity of AZD0530, a Src inhibitor, in pancreatic cancer. Clin Cancer Res. 2009;15:4138–46.

17. Pitts TM, Tan AC, Kulikowski GN, Tentler JJ, Brown AM, Flanigan SA, et al. Development of an integrated genomic classifier for a novel agent in colorectal cancer: approach to individualized therapy in early development. Clin Cancer Res. 2010;16:3193–204.

18. Rubio-Viqueira B, Jimeno A, Cusatis G, Zhang X, Iacobuzio-Donahue C, Karikari C, et al. An in vivo platform for translational drug development in pancreatic cancer. Clin Cancer Res. 2006;12:4652–61.

19. Tentler JJ, Tan AC, Weekes CD, Jimeno A, Leong S, Pitts TM, et al. Patient-derived tumour xenografts as models for oncology drug development. Nat Rev Clin Oncol. 2012;9:338–50.

20. Nguyen T, Carrieri FA, Connis N, Lafargue A, Chang J, Chan A, et al. TNIK inhibition sensitizes TNIK-overexpressing lung squamous cell carcinoma to radiotherapy. Mol Cancer Ther. 2024;23:1201–11.

21. Masuda M, Uno Y, Ohbayashi N, Ohata H, Mimata A, Kukimoto-Niino M, et al. TNIK inhibition abrogates colorectal cancer stemness. Nat Commun. 2016;7:12586.

22. Mahmoudi T, Li VSW, Ng SS, Taouatas N, Vries RGJ, Mohammed S, et al. The kinase TNIK is an essential activator of Wnt target genes. EMBO J. 2009;28:3329–40.

23. Lee RS, Zhang L, Berger A, Lawrence MG, Song J, Niranjan B, et al. Characterization of the ERG-regulated Kinome in Prostate Cancer Identifies TNIK as a Potential Therapeutic Target. Neoplasia. 2019;21:389–400.

24. Yu D-H, Zhang X, Wang H, Zhang L, Chen H, Hu M, et al. The essential role of TNIK gene amplification in gastric cancer growth. Oncogenesis. 2014;2:e89.

25. Torres-Ayuso P, An E, Nyswaner KM, Bensen RC, Ritt DA, Specht SI, et al. TNIK Is a Therapeutic Target in Lung Squamous Cell Carcinoma and Regulates FAK Activation through Merlin. Cancer Discov. 2021;11:1411–23.

26. Zhou K, Cheong JE, Krishnaji ST, Ghalali A, Fu H, Sui L, et al. Inhibition of Wnt Signaling in Colon Cancer Cells via an Oral Drug that Facilitates TNIK Degradation. Mol Cancer Ther. 2023;22:25–36.

27. Lee Y, Jung J-I, Park K-Y, Kim SA, Kim J. Synergistic inhibition effect of TNIK inhibitor KY-05009 and receptor tyrosine kinase inhibitor dovitinib on IL-6-induced proliferation and Wnt signaling pathway in human multiple myeloma cells. Oncotarget. 2017;8:41091–101.

28. Sato K, Padgaonkar AA, Baker SJ, Cosenza SC, Rechkoblit O, Subbaiah DRCV, et al. Simultaneous CK2/TNIK/DYRK1 inhibition by 108600 suppresses triple negative breast cancer stem cells and chemotherapy-resistant disease. Nat Commun. 2021;12:4671.

29. Yamada T, Masuda M. Emergence of TNIK inhibitors in cancer therapeutics. Cancer Sci. 2017;108:818–23.

30. Shkoda A, Town JA, Griese J, Romio M, Sarioglu H, Knöfel T, et al. The germinal center kinase TNIK is required for canonical NF-κB and JNK signaling in B-cells by the EBV oncoprotein LMP1 and the CD40 receptor. PLoS Biol. 2012;10:e1001376.

31. Sun Y, Gao X, Wu P, Wink M, Li J, Dian L, et al. Jatrorrhizine inhibits mammary carcinoma cells by targeting TNIK mediated Wnt/β-catenin signalling and epithelial-mesenchymal transition (EMT). Phytomedicine. 2019;63:153015.

32. Hann CL, Daniel VC, Sugar EA, Dobromilskaya I, Murphy SC, Cope L, et al. Therapeutic efficacy of ABT-737, a selective inhibitor of BCL-2, in small cell lung cancer. Cancer Res. 2008;68:2321–8.

33. Poirier JT, Dobromilskaya I, Moriarty WF, Peacock CD, Hann CL, Rudin CM. Selective tropism of Seneca Valley virus for variant subtype small cell lung cancer. J Natl Cancer Inst. 2013;105:1059–65.

34. Wong J, Armour E, Kazanzides P, Iordachita I, Tryggestad E, Deng H, et al. High-resolution, small animal radiation research platform with x-ray tomographic guidance capabilities. Int J Radiat Oncol Biol Phys. 2008;71:1591–9.

35. Zeng J, Aziz K, Chettiar ST, Aftab BT, Armour M, Gajula R, et al. Hedgehog pathway inhibition radiosensitizes non-small cell lung cancers. Int J Radiat Oncol Biol Phys. 2013;86:143–9.

36. Patro R, Duggal G, Love MI, Irizarry RA, Kingsford C. Salmon provides fast and bias-aware quantification of transcript expression. Nat Methods. 2017;14:417–9.

37. Soneson C, Love MI, Robinson MD. Differential analyses for RNA-seq: transcript-level estimates improve gene-level inferences. F1000Res. 2015;4:1521.

38. Robinson MD, Oshlack A. A scaling normalization method for differential expression analysis of RNA-seq data. Genome Biol. 2010;11:R25.

39. Ritchie ME, Phipson B, Wu D, Hu Y, Law CW, Shi W, et al. limma powers differential expression analyses for RNA-sequencing and microarray studies. Nucleic Acids Res. 2015;43:e47.

40. Law CW, Chen Y, Shi W, Smyth GK. voom: Precision weights unlock linear model analysis tools for RNA-seq read counts. Genome Biol. 2014;15:R29.

41. Hedges LV. Distribution Theory for Glass's Estimator of Effect Size and Related Estimators. Journal of Educational Statistics. [Sage Publications, Inc., American Educational Research Association, American Statistical Association]; 1981;6:107–28.

42. Wu D, Lim E, Vaillant F, Asselin-Labat M-L, Visvader JE, Smyth GK. ROAST: rotation gene set tests for complex microarray experiments. Bioinformatics. 2010;26:2176–82.

43. Chou T-C. Drug combination studies and their synergy quantification using the Chou-Talalay method. Cancer Res. 2010;70:440–6.

44. Zheng S, Wang W, Aldahdooh J, Malyutina A, Shadbahr T, Tanoli Z, et al. SynergyFinder Plus: Toward Better Interpretation and Annotation of Drug Combination Screening Datasets. Genomics Proteomics Bioinformatics. 2022;20:587–96.

45. Yadav B, Wennerberg K, Aittokallio T, Tang J. Searching for Drug Synergy in Complex Dose-Response Landscapes Using an Interaction Potency Model. Comput Struct Biotechnol J. 2015;13:504–13.

46. Ianevski A, Giri AK, Aittokallio T. SynergyFinder 2.0: visual analytics of multi-drug combination synergies. Nucleic Acids Res. 2020;48:W488–93.

47. Franken NAP, Rodermond HM, Stap J, Haveman J, van Bree C. Clonogenic assay of cells in vitro. Nat Protoc. 2006;1:2315–9.

48. Wang X, Raman N, Lemtiri-Chlieh G, Chang J, Jagtap S, Chowdhury DD, et al. Griseofulvin Radiosensitizes Non-Small Cell Lung Cancer Cells and Activates cGAS. Mol Cancer Ther. 2023;22:519–28.

49. Schultz CW, Zhang Y, Elmeskini R, Zimmermann A, Fu H, Murai Y, et al. ATR inhibition augments the efficacy of lurbinectedin in small-cell lung cancer. EMBO Mol Med. 2023;15:e17313.

50. Vakifahmetoglu H, Olsson M, Zhivotovsky B. Death through a tragedy: mitotic catastrophe. Cell Death Differ. 2008;15:1153–62.

51. Taparra K, Wang H, Malek R, Lafargue A, Barbhuiya MA, Wang X, et al. O-GlcNAcylation is required for mutant KRAS-induced lung tumorigenesis. J Clin Invest. 2018;128:4924–37.

52. Rudin CM, Durinck S, Stawiski EW, Poirier JT, Modrusan Z, Shames DS, et al. Comprehensive genomic analysis identifies SOX2 as a frequently amplified gene in small-cell lung cancer. Nat Genet. 2012;44:1111–6.

53. George J, Lim JS, Jang SJ, Cun Y, Ozretić L, Kong G, et al. Comprehensive genomic profiles of small cell lung cancer. Nature. 2015;524:47–53.

54. Pud D, Har-Zahav G, Laitman Y, Rubinek T, Yeheskel A, Ben-Ami S, et al. Association between variants of 5-hydroxytryptamine receptor 3C (HTR3C) and chemotherapy-induced symptoms in women receiving adjuvant treatment for breast cancer. Breast Cancer Res Treat. 2014;144:123–31.

55. Jahchan NS, Dudley JT, Mazur PK, Flores N, Yang D, Palmerton A, et al. A drug repositioning approach identifies tricyclic antidepressants as inhibitors of small cell lung cancer and other neuroendocrine tumors. Cancer Discov. 2013;3:1364–77.

Figure Legends

Figure 1: PDXs can be used to model and identify targets to combat rapid chemoradiation resistance in LS-SCLC. LX33 PDXs were treated, tumors collected at maximal tumor response, and gene expression profiles obtained across groups. (A) Schematic representation of experimental design for RNA profiling starting from PDX injection, followed by randomizing PDX tumor-bearing mice into 4 treatment arms, and finally collecting samples for RNA profiling. (B) Tumor volumes in LX33 PDX in response to vehicle (n=4), CT (n=5), RT (n=4), and CRT (n=4) treatments. One-way Anova with Tukey's multiple comparison's test, ns: nonsignificant; $*P < 0.05$, $**P < 0.01$, $***P < 0.001$, $****P < 0.0001$. (C) UpSet plot for differentially expressed genes (FDR < 10%) between treatment groups and control. The dots at the bottom of the plot represent the intersection between the groups, the bars on top are the number of genes in each intersection, and the bars on the right panel next to the dots are the total number of differentially expressed (DE) genes in each treatment arm. Data obtained from RNA profiling of the control (collected at day 6) and treatment (collected at day 12) samples. (D) Chemoradiation resistance candidate genes as identified from the LX33 SCLC PDX and human studies combined.

Figure 2: TNIK is identified as a chemoradiation resistance candidate gene in multiple SCLC PDXs with increased TNIK expression in the chemoradiation-resistant population of cells. (A) Schematic representation of experimental design for RNA-seq starting from PDX injection, followed by randomizing PDX tumor-bearing mice into 4 treatment arms, and finally collecting samples for RNA-seq (B) IHC showing the different molecular subtypes of SCLC PDX. (C) Tumor volumes in multiple SCLC PDX models in response to vehicle, CT, RT, and CRT treatments. Green dotted lines indicate the timepoints when the samples were collected: day 14 (early) and day 43 (late). Data are shown for 5–8 mice per treatment group per PDX model at the late timepoint. One-way ANOVA with Tukey HSD correction, ns, nonsignificant; $*P < 0.05$, $**P < 0.01$, $***P < 0.001$, $****P < 0.0001$. (D) PCA clustering of RNA-seq data of 5 PDXs (LU86, LU148, LX47, LU73 and LX33) exposed to vehicle, CT, RT, and combination (CRT) treatments. (E) Volcano plot showing the differentially expressed genes in all PDXs in the chemoradiation (CRT) resistant subpopulation of cancer cells. (F) TNIK expression in the different SCLC PDX models in response to vehicle, CT, RT, and CRT treatments. One-way ANOVA with Tukey HSD correction, ns, nonsignificant; $*P < 0.05$, $**P < 0.01$, $***P < 0.001$, $****P < 0.0001$.

Figure 3: TNIK inhibition sensitizes $TNIK^{high}$ SCLC cells to chemoradiation but not $TNIK^{low}$ cells. (A) TNIK expression in different SCLC cell lines (H446, H196, DMS114, H2286) as obtained from CCLE (https://depmap.org/portal/gene/TNIK?tab=characterization) and analyzed by Western blot. LK2 is a positive control and KNS62 is a negative control for TNIK expression. (B) Short-term cell viability of SCLC cell lines (H446, DMS114) in response to NCB-0846, determined with CellTiter-Glo 2.0 assay. EC50 was calculated on GraphPad Prism 10.0 using non-linear regression log(inhibitor) vs response variable slope (four parameters) (C) Clonogenic survival of $TNIK^{high}$ (H446) and $TNIK^{low}$ (DMS114) cells pre-treated with ethanol vs. NCB-0846 (300 nM, 48h) in response to IR at indicated doses. The image is representative of three independent experiments. Two-way Anova with Tukey's multiple comparison's test, ns: nonsignificant; $*P < 0.05$, $**P < 0.01$, $***P < 0.001$,

****$P < 0.0001$. (D) Clonogenic survival of TNIK^{high} (H446) cells exposed to IR (at all indicated doses) post-transfection with TNIK siRNA or scramble control. Data is representative of three independent experiments. Two-way Anova with Tukey's multiple comparison's test, ns: nonsignificant; *$P < 0.05$, **$P < 0.01$, ***$P < 0.001$, ****$P < 0.0001$. (E) Clonogenic survival of TNIK-overexpressing vs. mCherry-overexpressing DMS114 cells in response to IR at all indicated doses. Stable cell lines were generated via lentiviral transduction. TNIK overexpression was verified with a Western blot. Data is representative of three independent experiments. Two-way Anova with Tukey's multiple comparison's test, ns: nonsignificant; *$P < 0.05$, **$P < 0.01$, ***$P < 0.001$, ****$P < 0.0001$.

Figure 4: TNIK inhibition impairs the DNA damage response in TNIK^{high} SCLC cells exposed to radiation. (A) Activation status of DDR proteins (γH2AX, ATM/p-ATM, ATR/p-ATR, Chk1/p-Chk1, Chk2/p-Chk2) in TNIK^{high} H446 cells and TNIK^{low} DMS114 cells pre-treated with ethanol vs. NCB-0846 (300 nM, 1h and 24h) post-IR (6 Gy) as determined by immunoblotting. Cell lysates were collected at 1h and 24h post-IR. (B) Comet assay fluorescence imaging of H446 nucleoids at 24 hrs post-treatment with ethanol vs NCB-0846 (300 nM) with or without IR (6 Gy). Evaluation of the tail moment of nucleoids from H446 cells at 24 hrs following treatment with either ethanol or NCB-0846 (300 nM) with and without IR (6 Gy and 10 Gy). One-way Anova with Tukey's multiple comparison's test, ns: nonsignificant; *$P < 0.05$, **$P < 0.01$, ***$P < 0.001$, ****$P < 0.0001$. (C) Cell cycle distribution of TNIK^{high} H446 cells and TNIK^{low} DMS114 cells pretreated with ethanol vs NCB-0846 (300 nM, 24h) post-IR. Two-way Anova with Tukey's multiple comparison's test, ns: nonsignificant; *$P < 0.05$, **$P < 0.01$, ***$P < 0.001$, ****$P < 0.0001$. (D) Nuclear morphology of H446 cells treated with either vehicle or NCB-0846 (300 nM) with and without IR. Frequency of mitotic catastrophe in TNIK^{high} H446 and TNIK^{low} DMS114 cells treated with ethanol vs. NCB-0846 (300 nM, 24h) post-IR (6 Gy). Multi-nucleated cells were assessed as having undergone mitotic catastrophe. One-way Anova with Tukey's multiple comparison's test, ns: nonsignificant; *$P < 0.05$, **$P < 0.01$, ***$P < 0.001$, ****$P < 0.0001$. Data is representative of three independent experiments. Immunoblot band intensity was quantified with ImageJ.

Figure 5: TNIK inhibition promotes chemoradiotherapy sensitivity *in vivo* in SCLC xenograft tumors. (A) Schematic of *in vivo* studies showing the chemoradiation sensitizing potential of TNIKi. (B) TNIK expression in LX33 and H446 tumors (3 different mice, respectively) as determined by Western blot. (C) Tumor volumes in the LX33 PDX and H446 CDX models in response to vehicle (control), NCB-0846 (TNIKi), chemoradiation (CRT) and chemoradiation plus NCB-0846 (CRT+ TNIKi) treatments. Two-way Anova with Tukey's multiple comparison's test, ns: nonsignificant; *$P < 0.05$, **$P < 0.01$, ***$P < 0.001$, ****$P < 0.0001$. (D) Mouse body weight from all treatment groups over time in both LX33 PDX and H446 CDX.

Fig 1

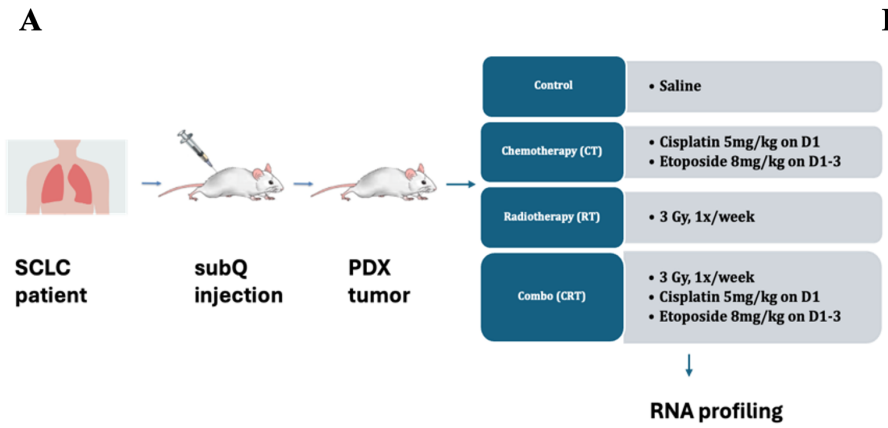

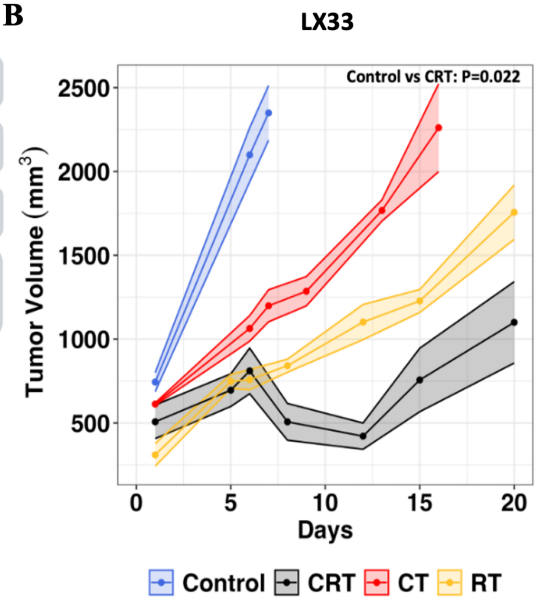

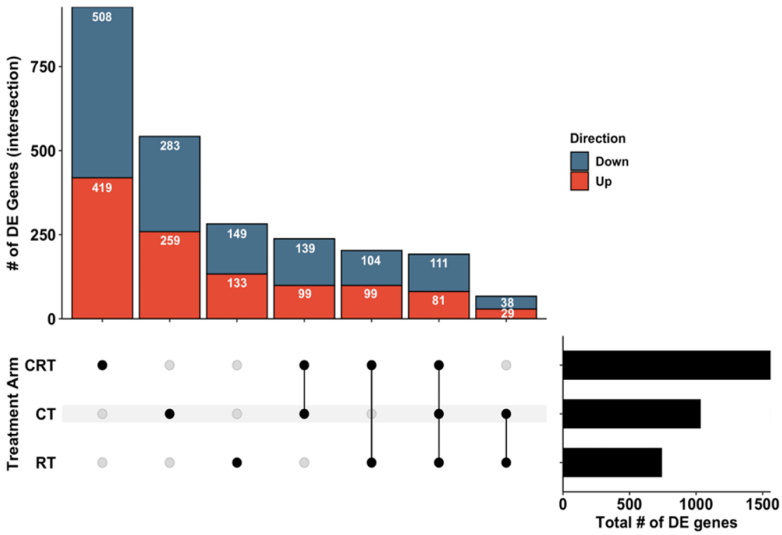

D

Genes upregulated in LX33 PDX and amplified in Rudin and George cohorts

Genes	Function	In vivo modulation
TNIK (Traf2 and Nck-interacting kinase)	First in-class anti-cancer target which is a potent activator of Wnt signaling and EMT regulator	NCB-0846 (Small molecule Wnt inhibitor)
HTR3C	A subunit of the 5-HT3 serotonin receptor	Citalopram

Fig 2

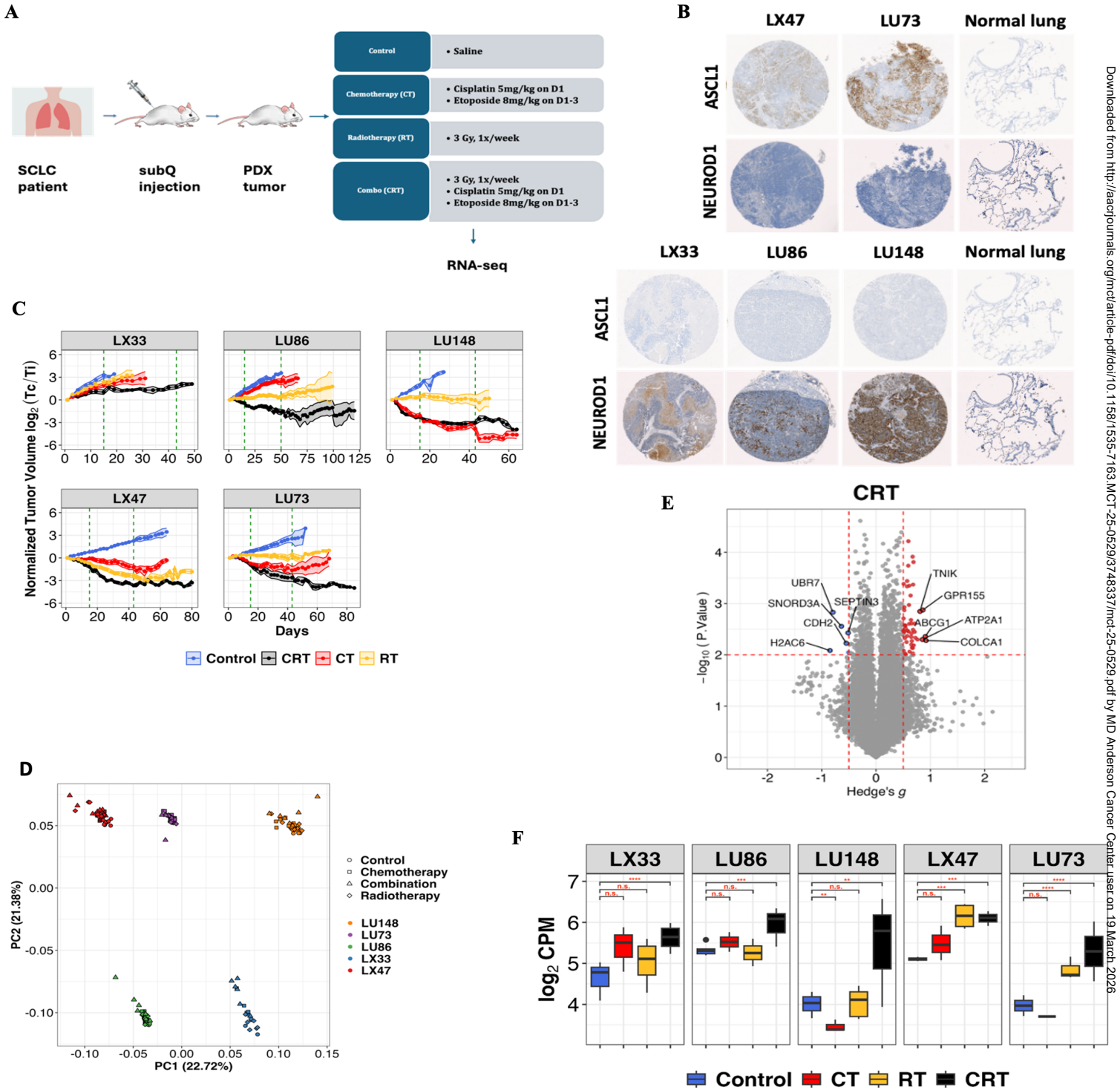

Fig 3

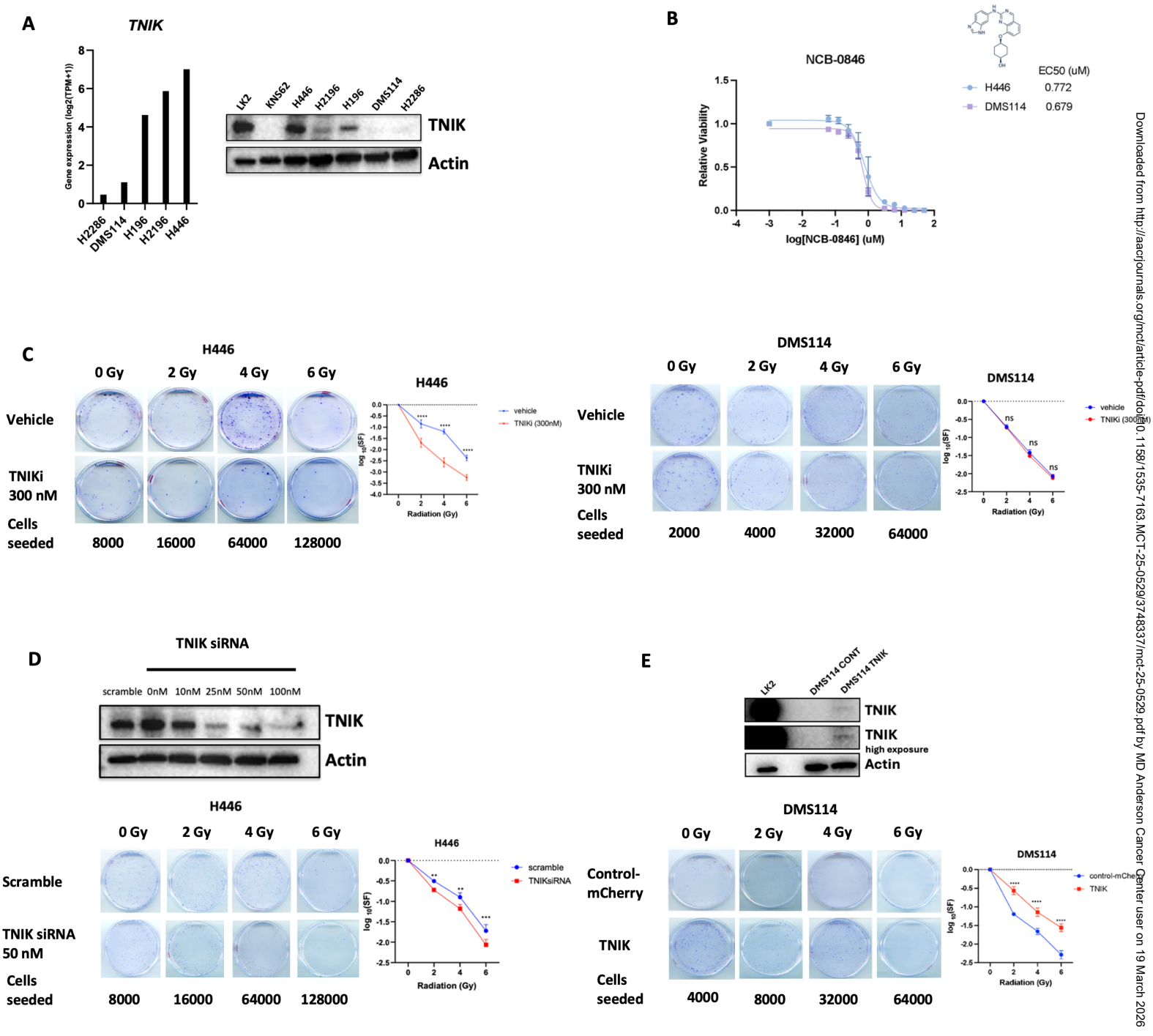

Fig 4

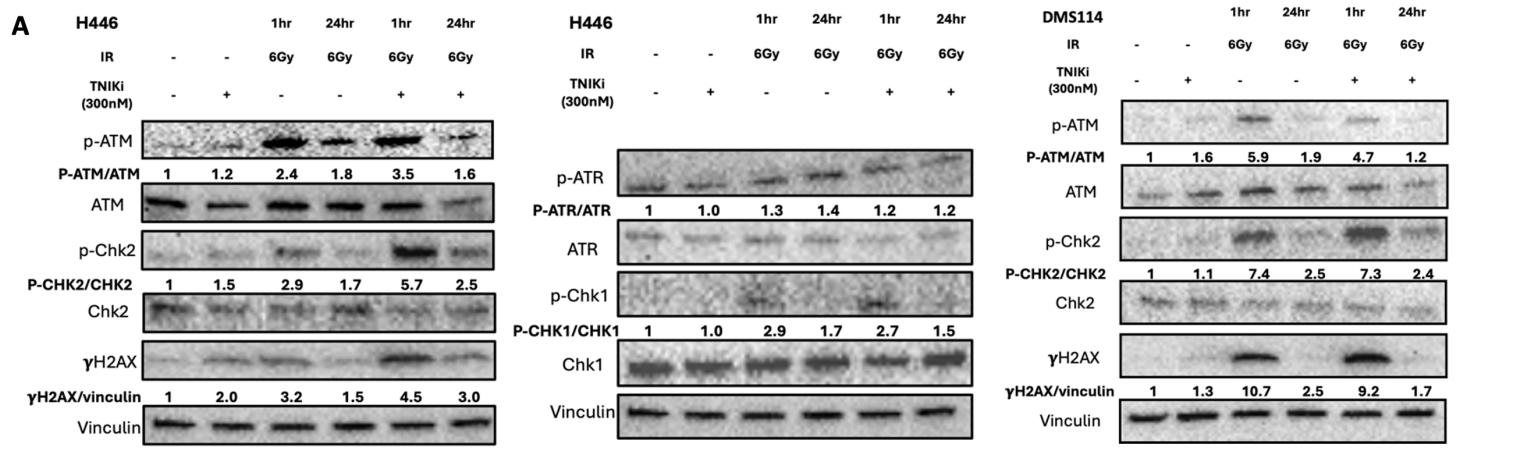

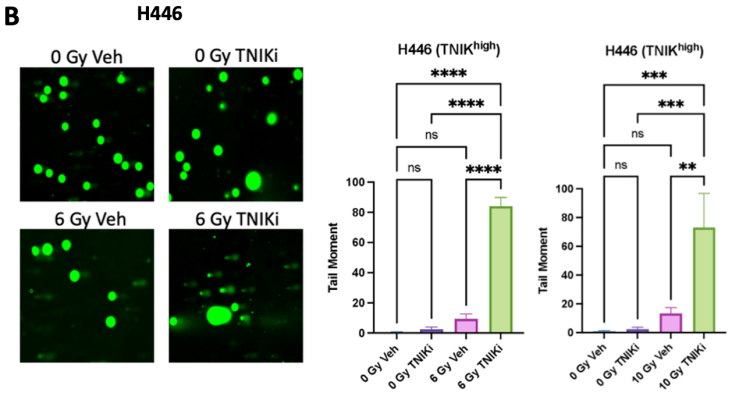

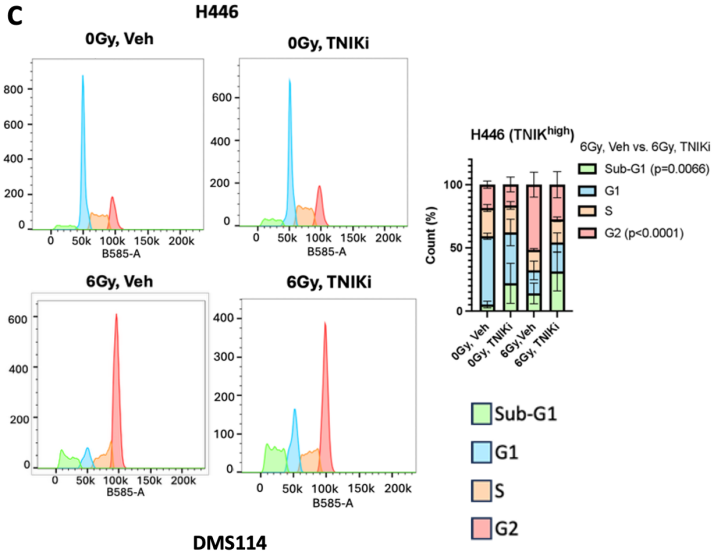

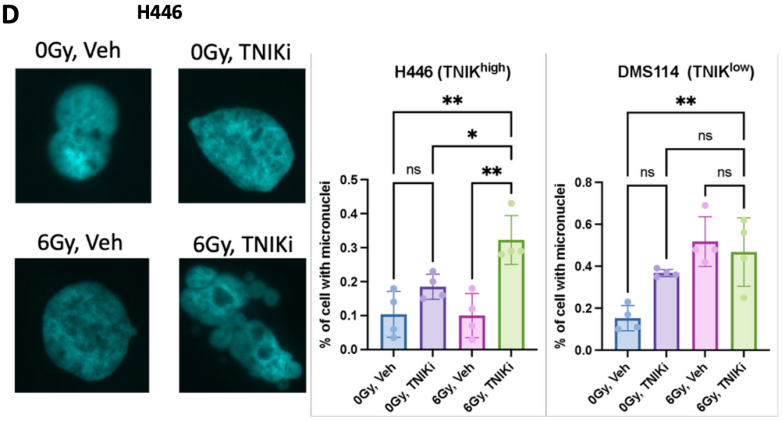

Fig 5